

Majorana Stripe Order on the Surface of a Three-Dimensional Topological Insulator

Y. Kamiya,^{1,*} A. Furusaki,¹ J. C. Y. Teo,² and G.-W. Chern^{2,†}

¹Condensed Matter Theory Laboratory, RIKEN, Wako, Saitama 351-0198, Japan

²Department of Physics, University of Virginia, Charlottesville, VA 22904, USA

(Dated: January 27, 2023)

The effect of interactions in topological states is a topical issue that includes not only interacting topological phases but also novel symmetry-breaking phases and phase transitions. Here we study the interaction effect on Majorana zero modes (MZMs) manifested on a vortex lattice in 2D topological superconductors. Under a special neutrality condition, where single-body hybridization between MZMs is prohibited by an emergent symmetry, we show that a minimal model for MZMs can be faithfully mapped to a quantum spin model, which has no sign problem in the world-line quantum Monte Carlo simulation. Guided by an insight from a further duality mapping to a compass model, we demonstrate that the interaction induces a *Majorana stripe order* spontaneously breaking translational and rotational symmetries. Away from neutrality, a mean-field theory suggests a quantum critical point induced by hybridization, beyond which a Dirac cone appears in the excitation spectrum.

Topological states of matter have been the focus of research during the last decade [1–3]. In this rapid development, bulk-boundary correspondence has been a central guiding principle, which predicts low-energy modes at the interface between topologically distinct states. The same principle also applies to topological defects (such as dislocations and superconducting vortices) in topological matters, because they can be regarded as generalized interfaces bordering on normal states [4–8]. Of particular interest are *Majorana zero modes* (MZMs), which are predicted to emerge at vortices in 2D topological superconductors, because of their potential for quantum computation [9–18]. Meanwhile, designing lattices of Majorana fermions out of MZMs is fascinating in its own right, because interaction between MZMs may lead to novel phases and critical phenomena [19–24].

In this Letter, we study a square lattice of interacting MZMs, which may emerge at vortices in 2D topological superfluid and superconductor [25–27], as was predicted for the *A* phase of ³He and Sr₂RuO₄ [28–30]. Here, we consider a surface of a 3D strong topological insulator (TI) subject to superconducting proximity effect, motivated by the proposed tunability of the system between weak- and strong-coupling regimes [21, 22]. Our choice of this platform is also motivated by recent experimental progress [31]. In a seminal work [12], Fu and Kane predicted that the superconducting topological surface state resembles a spinless $p_x \pm ip_y$ superconductor. When an Abrikosov vortex lattice is induced by a magnetic field, MZMs are expected to emerge at vortices [5], leading to a novel lattice of Majorana fermions at low energies. Here we assume additional conditions, such as strong fourfold lattice anisotropy, to stabilize a square vortex lattice as in LuNi₂B₂C [32]. Besides being one of the simplest structures, the reason for considering the square lattice is that a minimal Hamiltonian in the neutrality condition [21, 22] admits a faithful spin representation. This allows for employing a powerful quantum Monte Carlo (QMC) method [33] to investigate thermodynamic properties. In particular, we find a novel “Majorana stripe” phase. We show that a duality transformation provides an essential insight to elucidate the nature of this phase. With this solid understand-

ing, we also investigate the system away from neutrality by a mean-field (MF) theory. We find a quantum critical point induced by Majorana hybridization, beyond which a Dirac cone appears in the excitation spectrum.

At the non-interacting level, the system is described by the Fu-Kane Hamiltonian [12] $\hat{H}_{\text{FK}} = \frac{1}{2} \int d^2\mathbf{r} \hat{\Psi}_{\mathbf{r}}^\dagger \mathcal{H}_{\text{FK}}(\mathbf{r}) \hat{\Psi}_{\mathbf{r}}$ with $\hat{\Psi}_{\mathbf{r}} = (\hat{\psi}_{\uparrow\mathbf{r}}, \hat{\psi}_{\downarrow\mathbf{r}}, \hat{\psi}_{\downarrow\mathbf{r}}^\dagger, -\hat{\psi}_{\uparrow\mathbf{r}}^\dagger)^T$ being the Nambu spinor of the electronic operators $\hat{\psi}_{\sigma\mathbf{r}}^{(\dagger)}$ ($\sigma = \uparrow, \downarrow$) and

$$\mathcal{H}_{\text{FK}}(\mathbf{r}) = \tau^z (-iv_F \boldsymbol{\sigma} \cdot \nabla - \mu_F) + \text{Re} \Delta(\mathbf{r}) \tau^x + \text{Im} \Delta(\mathbf{r}) \tau^y, \quad (1)$$

where σ (τ) is the Pauli matrix in the spin (Nambu) basis, μ_F is the chemical potential, $\Delta(\mathbf{r})$ is the proximity-induced pair potential, and v_F is velocity of the surface Dirac mode when $\Delta = 0$. The distribution and the structure of vortices are encoded in $\Delta(\mathbf{r})$ and MZMs can be obtained by solving Eq. (1) [21]. The neutrality condition $\mu_F = 0$ has a significant consequence on the emergent symmetry of an effective Hamiltonian of MZMs. When satisfied, an artificial time-reversal symmetry $\hat{\Theta}_{\text{eff}} = \sigma^x \tau^x K$ (K is the complex conjugation) with $\hat{\Theta}_{\text{eff}}^2 = 1$ emerges in addition to the particle-hole symmetry $\Xi = \sigma^y \tau^y K$ inherent to the Bogoliubov-de Gennes formalism. The consequence is that MZMs do not mix different spins, and those bounded to vortices are spin-down states: $\hat{\gamma}_{\mathbf{r}} = u_{\mathbf{r}} \hat{\psi}_{\downarrow\mathbf{r}} + u_{\mathbf{r}}^* \hat{\psi}_{\downarrow\mathbf{r}}^\dagger$ [22]. Because $\hat{\Theta}_{\text{eff}} \hat{\gamma}_{\mathbf{r}} \hat{\Theta}_{\text{eff}}^{-1} = \hat{\gamma}_{\mathbf{r}}$ and $\hat{\Theta}_{\text{eff}}$ is antiunitary, single-body hybridizations $i\hat{\gamma}_{\mathbf{r}}\hat{\gamma}_{\mathbf{r}'}$ are prohibited at $\mu_F = 0$ between MZMs. For an interacting many-body system, this suggests that the neutrality condition corresponds to the *strong coupling limit* for the Majorana modes. Assuming the simplest, most local and quartic interaction of the vortex Majorana modes on the square lattice, we consider

$$\hat{H}_g = g \sum_{\square} \hat{\gamma}_{\square_1} \hat{\gamma}_{\square_2} \hat{\gamma}_{\square_3} \hat{\gamma}_{\square_4}, \quad (2)$$

where $\hat{\gamma}_{\mathbf{r}}$ is the Majorana fermion operator at site \mathbf{r} satisfying $\hat{\gamma}_{\mathbf{r}}^\dagger = \hat{\gamma}_{\mathbf{r}}$ and $\{\hat{\gamma}_{\mathbf{r}}, \hat{\gamma}_{\mathbf{r}'}\} = 2\delta_{\mathbf{r},\mathbf{r}'}$ and the summation runs over elementary plaquettes of the square lattice; $\square_1 - \square_4$ are four corners of a plaquette, $\square_2 = \square_1 - \mathbf{b}$, $\square_3 = \square_1 + \mathbf{a}$, and $\square_4 = \square_3 - \mathbf{b}$, with \mathbf{a} and \mathbf{b} the primitive lattice vectors [Fig. 1(a)].

Away from the neutrality condition, where hybridization terms are allowed, we consider $\hat{H} = \hat{H}_g + \hat{H}_t$ with

$$\hat{H}_t = it \sum_{\mathbf{r}} [\hat{\gamma}_{\mathbf{r}} \hat{\gamma}_{\mathbf{r}-\mathbf{b}} + (-1)^{r_y} \hat{\gamma}_{\mathbf{r}} \hat{\gamma}_{\mathbf{r}+\mathbf{a}}], \quad (3)$$

which has a gauge-invariant π flux per plaquette because of the underlying vortices [21]. By continuity, we expect $|t| \ll |g|$ for small μ_F . In other words, the Fermi level is expected to serve as an experimental control of $|t/g|$ [21]. We assume $g, t > 0$ below unless otherwise mentioned.

We start from the many-body Majorana Hamiltonian in the neutrality condition, $\hat{H} = \hat{H}_g$. Assuming a periodic (open) boundary condition in the \mathbf{a} (\mathbf{b}) direction, we map it to a quantum spin model by using a 2D Jordan-Wigner (JW) transformation. We define a spinless complex fermion $\hat{c}_{\mathbf{r}_\sigma} = \frac{1}{2}(\hat{\gamma}_{\mathbf{r}_{\sigma,1}} + i\hat{\gamma}_{\mathbf{r}_{\sigma,2}})$ by introducing pairings in the whole lattice, where \mathbf{r}_σ is the position of a dimer combining $\hat{\gamma}_{\mathbf{r}_{\sigma,1}}$ and $\hat{\gamma}_{\mathbf{r}_{\sigma,2}}$ at its end points [Fig. 1(b)]. Assuming the “column-major” index $n_{\text{CM}}(\mathbf{r}_\sigma)$ for dimers in Fig. 1(b), the transformation is $\hat{c}_{\mathbf{r}_\sigma}^\dagger \hat{c}_{\mathbf{r}_\sigma} = \frac{1}{2}(1 + \hat{\sigma}_{\mathbf{r}_\sigma}^z)$ and $\hat{c}_{\mathbf{r}_\sigma}^\dagger = \frac{1}{2}(\prod_{n_{\text{CM}}(\mathbf{r}'_\sigma) < n_{\text{CM}}(\mathbf{r}_\sigma)} \hat{\sigma}_{\mathbf{r}'_\sigma}^z) (\hat{\sigma}_{\mathbf{r}_\sigma}^x + i\hat{\sigma}_{\mathbf{r}_\sigma}^y)$, where $\hat{\sigma}^\alpha$ ($\alpha = x, y, z$) are the Pauli matrices. Depending on the number of dimers involved in a plaquette interaction (i.e., two or four), the interaction is transformed in a different way [Fig. 1(c)]:

$$\begin{aligned} \hat{\gamma}_{\mathbf{r}_{\sigma,2}} \hat{\gamma}_{\mathbf{r}_{\sigma,1}} \hat{\gamma}_{\mathbf{r}_{\sigma+\mathbf{a},2}} \hat{\gamma}_{\mathbf{r}_{\sigma+\mathbf{a},1}} &= -\hat{\sigma}_{\mathbf{r}_\sigma}^z \hat{\sigma}_{\mathbf{r}_\sigma+\mathbf{a}}^z, \\ \hat{\gamma}_{\mathbf{r}_{\sigma,1}} \hat{\gamma}_{\mathbf{r}_{\sigma,2}} \hat{\gamma}_{\mathbf{r}_{\sigma+\mathbf{a},1}} \hat{\gamma}_{\mathbf{r}_{\sigma+\mathbf{a},2}} &= -\hat{\sigma}_{\mathbf{r}_\sigma}^x \hat{\sigma}_{\mathbf{r}_\sigma+\mathbf{a}}^x \hat{\sigma}_{\mathbf{r}_\sigma+\mathbf{a}}^y \hat{\sigma}_{\mathbf{r}_\sigma}^y, \end{aligned} \quad (4)$$

where $\mathbf{r}'_\sigma = \mathbf{r}_\sigma + 2\mathbf{b}$. The string factor does not appear in either case because any plaquette operator comprises products of two Majorana operators at neighboring sites in the same column, and such composite objects behave as bosons. We obtain

$$\hat{H}_{g,\sigma} = -J \sum_{\mathbf{r}_\sigma} \hat{\sigma}_{\mathbf{r}_\sigma}^z \hat{\sigma}_{\mathbf{r}_\sigma+\mathbf{a}}^z - P \sum_{\square_\sigma} \left(\prod_{\mathbf{r}_\sigma \in \square_\sigma} \hat{\sigma}_{\mathbf{r}_\sigma}^x \right), \quad (5)$$

with $J = P = g$, which combines the Ising coupling J on the horizontal bonds and a transverse four-spin term P associated with plaquettes (\square_σ) of σ spins [Fig. 1(b)].

Remarkably, in the spin representation (5), we can apply a *bosonic* QMC method [33] to study the thermodynamic properties of MZMs *without a negative sign problem*. The directed-loop algorithm [34, 35] in the σ^x basis is used in our simulations. To reduce finite size effects, we use a trick of fictitious MZMs to simulate the lattice of Majorana fermions comprising an even number of plaquettes in the \mathbf{b} direction [36]. We investigated the spin lattices of $L \times L$ up to $L = 60$, which corresponds to $L \times (2L - 1)$ MZMs.

Figure 2(a) shows the specific heat $C = (1/L^2) \partial \langle \hat{H}_{g,\sigma} \rangle / \partial T$. In addition to the broad peak around $T \approx g$, it exhibits a size-dependent sharp anomaly at $T/g \approx 0.25$, indicating a second-order transition. This observation points to a symmetry breaking phase at low T , which contradicts with the previous conjecture of a topological quantum critical point [21].

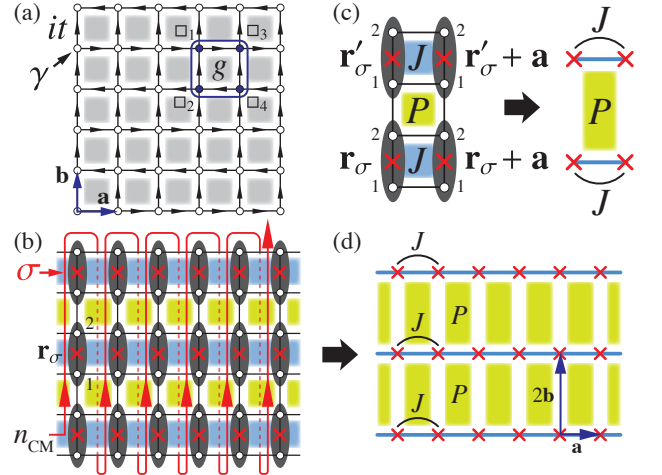


FIG. 1. MZMs and the JW transformation. (a) Square lattice of MZM, where plaquettes and directed links from site \mathbf{r} to site \mathbf{r}' represent the interaction g and the hybridization $it\hat{\gamma}_{\mathbf{r}}\hat{\gamma}_{\mathbf{r}'}$, respectively. (b) JW transformation of \hat{H}_g with the column-major site ordering n_{CM} . Ellipses show pairing of MZMs with crosses representing σ spins. (c) A plaquette term involving two (four) dimers is transformed to the Ising (four-spin) coupling, where $\mathbf{r}'_\sigma = \mathbf{r}_\sigma + 2\mathbf{b}$ (here $J = P = g$). (d) Lattice of σ spins.

However, we note that a long-range order of σ^z of any kind is impossible at $T > 0$ because of the presence of the gauge-like 1D symmetries; the string operator $\hat{O}_h^{\text{spin}}(y) = \prod_{\mathbf{r}_\sigma} \hat{\sigma}_{\mathbf{r}_\sigma}^x$, which flips σ^z eigenvalues of all spins in any horizontal chain, commutes with $\hat{H}_{g,\sigma}$. As a generalized Elitzur’s theorem, these symmetries reduce the effective dimensionality of the order parameter field σ^z from 2D to 1D [37]. Hence, the corresponding 1D physics may explain the broad peak of C at high T , but not the transition itself.

To elucidate the nature of the low- T phase and the transition, we invoke a duality mapping. With a two-step Kramers-Wannier transformation [38], we show that $\hat{H}_{g,\sigma}$ (hence, \hat{H}_g) is dual to two decoupled copies of a square-lattice *quantum compass model* [39], which was investigated in depth in various contexts [40–50]. First, we define τ spins at the midpoint of every horizontal link. With the “row-major” site ordering $n_{\text{RM}}(\mathbf{r}_\sigma)$ in Fig. 3(a), the first transformation is $\hat{\tau}_{\mathbf{r}_\tau}^z = \hat{\sigma}_{\mathbf{r}_\sigma}^z \hat{\sigma}_{\mathbf{r}_\sigma+\mathbf{a}}^z$, $\hat{\tau}_{\mathbf{r}_\tau}^x = \prod_{n_{\text{RM}}(\mathbf{r}'_\sigma) \leq n_{\text{RM}}(\mathbf{r}_\sigma)} \hat{\sigma}_{\mathbf{r}'_\sigma}^x$ where $\mathbf{r}_\tau = \mathbf{r}_\sigma + \frac{\mathbf{a}}{2}$. The J and P terms become an effective magnetic field and a four-spin term for τ spins, respectively. We find that the latter does not mix τ spins in even and odd columns in the dual lattice, e.g., $\hat{\sigma}_{\mathbf{r}_\sigma}^x \hat{\sigma}_{\mathbf{r}_\sigma+\mathbf{a}}^x \hat{\sigma}_{\mathbf{r}_\sigma+2\mathbf{b}}^x \hat{\sigma}_{\mathbf{r}_\sigma+\mathbf{a}+2\mathbf{b}}^x = \hat{\tau}_{\mathbf{r}_\tau-\mathbf{a}}^x \hat{\tau}_{\mathbf{r}_\tau+\mathbf{a}}^x \hat{\tau}_{\mathbf{r}_\tau-\mathbf{a}+2\mathbf{b}}^x \hat{\tau}_{\mathbf{r}_\tau+\mathbf{a}+2\mathbf{b}}^x$ [Fig. 3(d)]. Consequently, the dual Hamiltonian $\hat{H}_{g,\tau} = \hat{H}_{g,\tau}^e + \hat{H}_{g,\tau}^o$ is composed of decoupled even and odd components,

$$\hat{H}_{g,\tau}^{e(o)} = \sum_{\mathbf{r}_\tau \in \text{even (odd) columns}} \left(-J \hat{\tau}_{\mathbf{r}_\tau}^z - P \hat{\tau}_{\mathbf{r}_\tau}^x \hat{\tau}_{\mathbf{r}_\tau+2\mathbf{a}}^x \hat{\tau}_{\mathbf{r}_\tau+2\mathbf{b}}^x \hat{\tau}_{\mathbf{r}_\tau+2\mathbf{a}+2\mathbf{b}}^x \right), \quad (6)$$

also known as the Xu-Moore model [46, 47]. In the second step, introducing μ spins at the midpoint of each vertical link

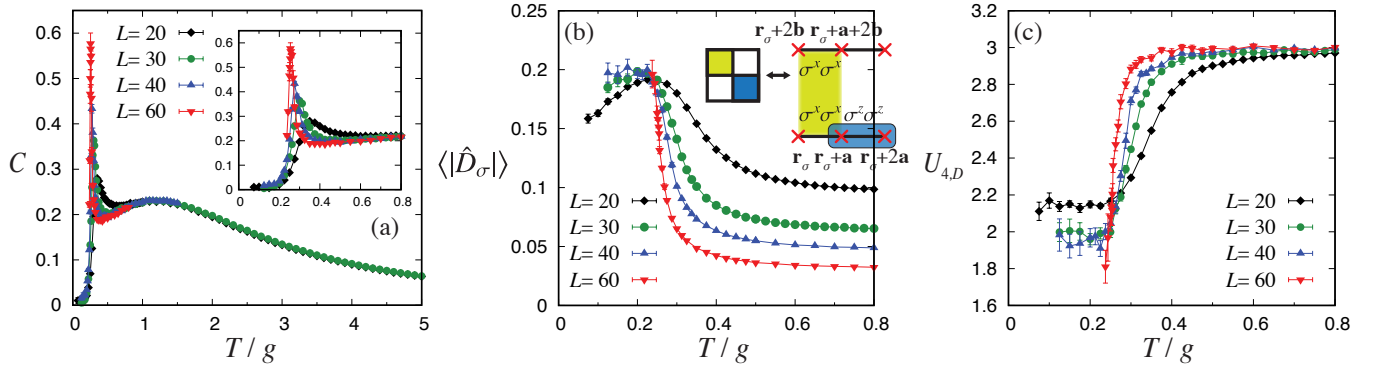


FIG. 2. QMC results in the spin representation (5) with $J = P = g$ in the $L \times L$ lattice with the fictitious MZM trick [36]. (a) Specific heat C , (b) the order parameter $\langle |\hat{D}_\sigma| \rangle$ of the Majorana stripe state, and (c) the Binder parameter. The inset in (b) illustrates the local order parameter $\hat{D}_\sigma(\mathbf{r}_\sigma)$ (8) and its relation with a pair of Majorana plaquettes.

$(\mathbf{r}_\tau, \mathbf{r}_\tau + 2\mathbf{b})$ for τ spins, the transformation is $\hat{\mu}_{\mathbf{r}_\mu}^x = \hat{\tau}_{\mathbf{r}_\tau}^x \hat{\tau}_{\mathbf{r}_\tau + 2\mathbf{b}}^x$, $\hat{\mu}_{\mathbf{r}_\mu}^z = \prod_{\tilde{n}_{\text{CM}}(\mathbf{r}'_\tau) \leq \tilde{n}_{\text{CM}}(\mathbf{r}_\tau)} \hat{\tau}_{\mathbf{r}'_\tau}^z$ with $\mathbf{r}_\mu = \mathbf{r}_\tau + \mathbf{b}$. $\tilde{n}_{\text{CM}}(\mathbf{r}_\tau)$ is the column-major ordering for τ spins [Fig. 3(b)]. This transformation preserves the decoupling of $\hat{H}_{g,\tau}^e$ and $\hat{H}_{g,\tau}^o$, transforming each into the quantum compass model defined as follows on a square lattice with an enlarged unit cell. We obtain [see Figs. 3(c)–3(e)],

$$\hat{H}_{g,\mu}^{e(o)} = \sum_{\mathbf{r}_\mu \in \text{even (odd) column}} \left(-P \hat{\mu}_{\mathbf{r}_\mu}^x \hat{\mu}_{\mathbf{r}_\mu + 2\mathbf{a}}^x - J \hat{\mu}_{\mathbf{r}_\mu}^z \hat{\mu}_{\mathbf{r}_\mu + 2\mathbf{b}}^z \right), \quad (7)$$

with the total Hamiltonian $\hat{H}_{g,\mu} = \hat{H}_{g,\mu}^e + \hat{H}_{g,\mu}^o$.

The above duality transformation provides a useful insight into the problem of $\hat{H} = \hat{H}_g$. The most crucial input from the compass model is that it undergoes a nematic transition at finite temperature, which belongs to the Ising universality class [40, 43, 44]. Below T_c , while any spin-spin correlation function such as $\langle \hat{\mu}_{\mathbf{r}_\mu}^x \hat{\mu}_{\mathbf{r}_\mu}^x \rangle$ and $\langle \hat{\mu}_{\mathbf{r}_\mu}^z \hat{\mu}_{\mathbf{r}_\mu}^z \rangle$ is short-ranged at $T > 0$, the \mathbb{Z}_2 reflection symmetry $x \leftrightarrow z$ ($\mathbf{a} \leftrightarrow \mathbf{b}$) in the spin (real) space is spontaneously broken, which can be detected by a directional order parameter $\hat{D}_\mu(\mathbf{r}_\mu) = \hat{\mu}_{\mathbf{r}_\mu}^x \hat{\mu}_{\mathbf{r}_\mu + 2\mathbf{a}}^x - \hat{\mu}_{\mathbf{r}_\mu}^z \hat{\mu}_{\mathbf{r}_\mu + 2\mathbf{b}}^z$ [39]. To translate this back to the language of Majorana fermions, we examine the correspondence of the operators between the two representations. First, the even-odd decomposition corresponds to the geometrical checkerboard decomposition of \hat{H}_g . Defining \hat{H}_g^A and \hat{H}_g^B as composed of quartic interactions associated with one sublattice of the checkerboard decomposition (A) and its complement (B), respectively, we find $\hat{H}_g = \hat{H}_g^A + \hat{H}_g^B$ [see Fig. 4(a)] and $[\hat{H}_g^A, \hat{H}_g^B] = 0$; \hat{H}_g^A corresponds to $\hat{H}_{g,\mu}^e$ or $\hat{H}_{g,\mu}^o$ and \hat{H}_g^B does to the other. Moreover, as demonstrated in the sequence of transformations, there is one-to-one correspondence between the quartic Majorana plaquette operators and the bond operators in the compass model. As illustrated in Fig. 4(a), each Ising-like bond interaction in $\hat{H}_{g,\mu}^{e(o)}$ (7) corresponds to a plaquette term that it overlaps. In this sense, the nematic order quantified by \hat{D}_μ can be understood as spontaneous *energy density modulation*. In the Majorana fermion

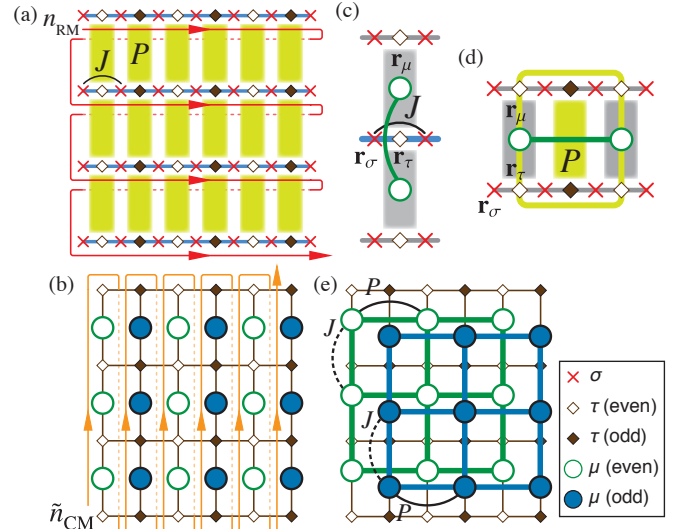


FIG. 3. Two-step duality transformation, introducing (a) τ spins and (b) μ spins. (c) The J term is transformed to the interaction in the vertical direction $\hat{\mu}_{\mathbf{r}_\mu}^z \hat{\mu}_{\mathbf{r}_\mu + 2\mathbf{b}}^z$. (d) The P term (highlighted filled rectangle) is transformed first into a four-spin coupling for τ spins (round rectangle) and then to the Ising interaction in the horizontal direction $\hat{\mu}_{\mathbf{r}_\mu}^x \hat{\mu}_{\mathbf{r}_\mu + 2\mathbf{a}}^x$. (e) Resulting decoupled copies of the quantum compass model for μ spins (shifted for clarity).

system, this is associated with the plaquette interaction g . As shown in Fig. 4(b), the even-odd decoupling means that the energy-density wave order emerges in the two sectors independently ($\mathbb{Z}_2 \times \mathbb{Z}_2$ symmetry breaking), resulting in fourfold degenerate ground states modulo 1D symmetries, which we call the *Majorana stripe order*.

We confirm this by evaluating the order parameter with QMC in the σ -spin representation. Figure 2(b) shows $\langle |\hat{D}_\sigma| \rangle$ with $\hat{D}_\sigma = \mathcal{N}^{-1} \sum_{\mathbf{r}_\sigma} \hat{D}_\sigma(\mathbf{r}_\sigma)$, where the summation runs over even or odd columns, \mathcal{N} is a proper normalization [36], and

$$\hat{D}_\sigma(\mathbf{r}_\sigma) = \hat{\sigma}_{\mathbf{r}_\sigma + \mathbf{a}}^z \hat{\sigma}_{\mathbf{r}_\sigma + 2\mathbf{a}}^z - \hat{\sigma}_{\mathbf{r}_\sigma + 2\mathbf{b}}^x \hat{\sigma}_{\mathbf{r}_\sigma}^x \hat{\sigma}_{\mathbf{r}_\sigma + \mathbf{a} + 2\mathbf{b}}^x \hat{\sigma}_{\mathbf{r}_\sigma + \mathbf{a}}^x. \quad (8)$$

We find that $\langle |D| \rangle$ becomes nearly size-independent at low

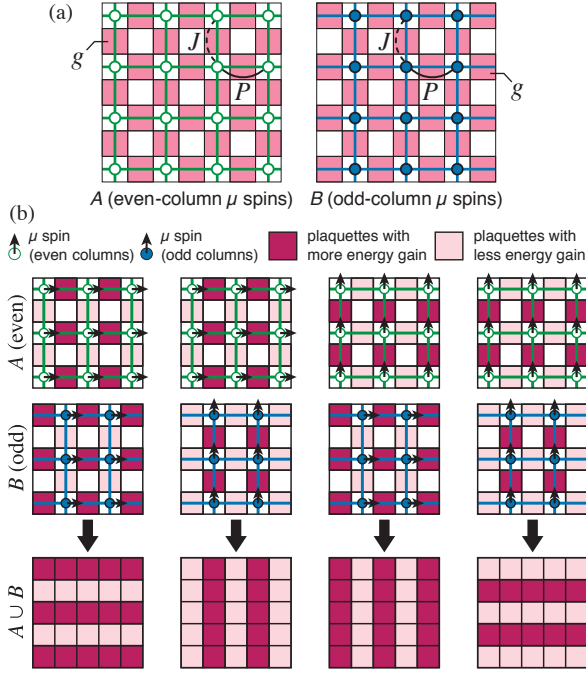


FIG. 4. Majorana stripe state. (a) Correspondence between the checkerboard decomposition of \hat{H}_g (2) and the even and odd components of the compass model. (b) Fourfold degenerate ordered state and the relation with the nematic order in the compass model.

T , confirming the Majorana stripe phase. The nonmonotonic T -dependence for small L is suggested to be a finite-size effect due to the open boundary condition in the y direction. Figure 2(c) shows the Binder parameter $U_{4,D} = \langle \hat{D}_\sigma^4 \rangle / \langle \hat{D}_\sigma^2 \rangle^2$, which exhibits crossing for different L at $T_c/g \approx 0.25(1)$, in agreement with the temperature of the divergent peak in C .

Finally, we address the effect of hybridization, \hat{H}_t (3), on the Majorana stripe phase. The finite temperature transition also implies a first-order transition line in the extended T - Δg phase diagram [Fig. 5(a)], where $\Delta g \equiv P - J$ denotes the perturbation that explicitly breaks the translational symmetry; see Fig. 1(c). Since the QMC method cannot be applied to $\hat{H}_g + \hat{H}_t$ due to the sign problem, we employ the MF method to examine the discontinuous transition at $T = 0$. Figure 5(b) shows the order parameter $D = \langle \hat{D}_\sigma \rangle$ as a function of Δg for varying values of hybridization t . A clear jump of D as $\Delta g \rightarrow 0$ for small t indicates that the discontinuous transition persists even in the presence of a weak hybridization. This in turn implies that the finite- T transition remains stable for small t . The hybridization induces a coupling between A and B subsystems, which may modify the universality class [51]. As t increases, the jump ΔD vanishes at a critical point $t_c \approx 0.65g$. The MF band structure of Majorana fermions at $\Delta g \rightarrow 0$ is shown in Fig. 5(c) for $t/g = 0.2, 0.8$. The spectrum in the stripe phase ($t < t_c$) is gapped with $\varepsilon_{\text{gap}} = \Delta D$, where the Chern number C is 0 [36]. The gap is reduced with increasing t and vanishes for $t > t_c$ as shown in Fig. 5(d). Assuming that the critical temperature $T_c \approx \varepsilon_{\text{gap}}$, our result suggests that T_c moves toward $T = 0$ with

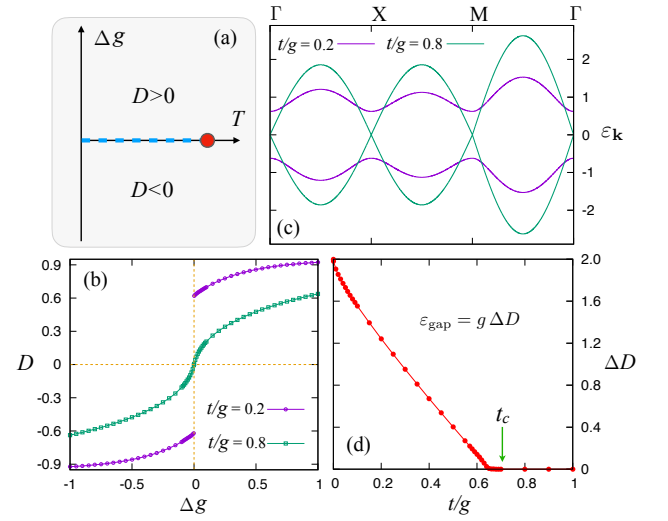


FIG. 5. MF results for $\hat{H}_t + \hat{H}_g$ (off neutrality). (a) Schematic phase diagram in the T - Δg plane showing a first-order transition line ending at finite- T critical point. (b) Stripe order parameter D as a function of Δg for $t/g = 0.2, 0.8$. (c) Majorana MF band structure for varying t . (d) Energy gap $\varepsilon_{\text{gap}}(t)$ for $\Delta g = 0$, which is equal to the jump ΔD of the stripe order parameter at $\Delta g = 0$ [36].

increasing hybridization. Our calculation thus points to the existence of a quantum critical point characterized by Dirac fermion excitations when $t \geq t_c$.

In summary, the square-lattice Majorana Hamiltonian $\hat{H}_t + \hat{H}_g$, which may have an experimental realization in the hybrid of a 3D strong TI and a superconductor, induces a stripe order that breaks the translational and rotational symmetries in the strong coupling regime $g \gg t$. Our QMC simulations as well as the duality mapping (via the JW transformation) to the compass model provide a solid confirmation of this phenomenon in the strong coupling limit. We note that Affleck *et al.* also investigated the same model recently, where it was suggested the transition $t = t_c$ belongs to a supersymmetric universality class based on a renormalization group theory [24]. Our approach coming from the strong coupling is complementary to their weak-coupling instability analysis. We hope that it will trigger an experimental effort in the search for intriguing phase transitions in the system of interacting Majorana modes.

We are grateful to Sharmistha Sahoo for useful discussions at the early stage of this project, and to Cristian Batista for valuable discussions. The numerical simulations in this work in part utilized the facilities of the Supercomputer Center, ISSP, the University of Tokyo. Y.K. acknowledges support by JSPS Grants-in-Aid for Scientific Research under Grant No. JP16H02206. A.F. acknowledge support by JSPS Grants-in-Aid for Scientific Research under Grant No. 15K05141. J.C.Y.T. is supported by the NSF under Grant No. DMR-1653535.

* yoshitomo.kamiya@riken.jp

† gchern@virginia.edu

- [1] M. Z. Hasan and C. L. Kane, *Rev. Mod. Phys.* **82**, 3045 (2010).
- [2] X.-L. Qi and S.-C. Zhang, *Rev. Mod. Phys.* **83**, 1057 (2011).
- [3] C.-K. Chiu, J. C. Y. Teo, A. P. Schnyder, and S. Ryu, *Rev. Mod. Phys.* **88**, 035005 (2016).
- [4] Y. Ran, Y. Zhang, and A. Vishwanath, *Nat. Phys.* **5**, 298 (2009).
- [5] J. C. Y. Teo and C. L. Kane, *Phys. Rev. B* **82**, 115120 (2010).
- [6] T. L. Hughes, H. Yao, and X.-L. Qi, *Phys. Rev. B* **90**, 235123 (2014).
- [7] J. C. Y. Teo and T. L. Hughes, *Phys. Rev. Lett.* **111**, 047006 (2013).
- [8] J. C. Teo and T. L. Hughes, *Annual Review of Condensed Matter Physics* **8**, 211 (2017).
- [9] A. Kitaev, *Ann. Phys.* **303**, 2 (2003).
- [10] C. Nayak, S. H. Simon, A. Stern, M. Freedman, and S. Das Sarma, *Rev. Mod. Phys.* **80**, 1083 (2008).
- [11] A. Kitaev, *Ann. Phys. (N.Y.)* **321**, 2 (2006).
- [12] L. Fu and C. L. Kane, *Phys. Rev. Lett.* **100**, 096407 (2008).
- [13] C. W. J. Beenakker, *Annu. Rev. Con. Mat. Phys.* **4**, 113 (2013).
- [14] J. Alicea, *Rep. Prog. Phys.* **75**, 076501 (2012).
- [15] T. D. Stanescu and S. Tewari, *J. Phys. Condens. Matter* **25**, 233201 (2013).
- [16] M. Leijnse and K. Flensberg, *Semicond. Sci. Technol.* **27**, 124003 (2012).
- [17] S. R. Elliott and M. Franz, *Rev. Mod. Phys.* **87**, 137 (2015).
- [18] S. Das Sarma, M. Freedman, and C. Nayak, *Npj Quantum Information* **1**, 15001 (2015).
- [19] A. Rahmani, X. Zhu, M. Franz, and I. Affleck, *Phys. Rev. Lett.* **115**, 166401 (2015).
- [20] A. Rahmani, X. Zhu, M. Franz, and I. Affleck, *Phys. Rev. B* **92**, 235123 (2015).
- [21] C.-K. Chiu, D. I. Pikulin, and M. Franz, *Phys. Rev. B* **91**, 165402 (2015).
- [22] C.-K. Chiu, D. I. Pikulin, and M. Franz, *Phys. Rev. B* **92**, 241115 (2015).
- [23] X. Zhu and M. Franz, *Phys. Rev. B* **93**, 195118 (2016).
- [24] I. Affleck, A. Rahmani, and D. Pikulin, *arXiv:1706.05469*.
- [25] G. E. Volovik, *Pisma Zh. Eksp. Teor. Fiz.* **70**, 601 (1999).
- [26] N. Read and D. Green, *Phys. Rev. B* **61**, 10267 (2000).
- [27] D. A. Ivanov, *Phys. Rev. Lett.* **86**, 268 (2001).
- [28] S. Das Sarma, C. Nayak, and S. Tewari, *Phys. Rev. B* **73**, 220502 (2006).
- [29] S. B. Chung, H. Bluhm, and E.-A. Kim, *Phys. Rev. Lett.* **99**, 197002 (2007).
- [30] J. Jang, D. G. Ferguson, V. Vakaryuk, R. Budakian, S. B. Chung, P. M. Goldbart, and Y. Maeno, *Science* **331**, 186 (2011).
- [31] J.-P. Xu, C. Liu, M.-X. Wang, J. Ge, Z.-L. Liu, X. Yang, Y. Chen, Y. Liu, Z.-A. Xu, C.-L. Gao, D. Qian, F.-C. Zhang, and J.-F. Jia, *Phys. Rev. Lett.* **112**, 217001 (2014).
- [32] Y. De Wilde, M. Iavarone, U. Welp, V. Metlushko, A. E. Koshelev, I. Aranson, G. W. Crabtree, and P. C. Canfield, *Phys. Rev. Lett.* **78**, 4273 (1997).
- [33] J. E. Gubernatis, N. Kawashima, and P. Werner, *Quantum Monte Carlo Methods* (Cambridge University Press, Cambridge, 2016).
- [34] O. F. Syljuåsen and A. W. Sandvik, *Phys. Rev. E* **66**, 046701 (2002).
- [35] F. Alet, S. Wessel, and M. Troyer, *Phys. Rev. E* **71**, 036706 (2005).

[36] See Supplemental Material for details.

- [37] C. D. Batista and Z. Nussinov, *Phys. Rev. B* **72**, 045137 (2005).
- [38] H. A. Kramers and G. H. Wannier, *Phys. Rev.* **60**, 252 (1941).
- [39] Z. Nussinov and J. van den Brink, *Rev. Mod. Phys.* **87**, 1 (2015).
- [40] A. Mishra, M. Ma, F.-C. Zhang, S. Guertler, L.-H. Tang, and S. Wan, *Phys. Rev. Lett.* **93**, 207201 (2004).
- [41] J. Dorier, F. Becca, and F. Mila, *Phys. Rev. B* **72**, 024448 (2005).
- [42] H.-D. Chen, C. Fang, J. Hu, and H. Yao, *Phys. Rev. B* **75**, 144401 (2007).
- [43] T. Tanaka and S. Ishihara, *Phys. Rev. Lett.* **98**, 256402 (2007).
- [44] S. Wenzel and W. Janke, *Phys. Rev. B* **78**, 064402 (2008).
- [45] R. Orús, A. C. Doherty, and G. Vidal, *Phys. Rev. Lett.* **102**, 077203 (2009).
- [46] C. Xu and J. E. Moore, *Phys. Rev. Lett.* **93**, 047003 (2004).
- [47] C. Xu and J. Moore, *Nucl. Phys. B* **716**, 487 (2005).
- [48] Z. Nussinov and E. Fradkin, *Phys. Rev. B* **71**, 195120 (2005).
- [49] J. Vidal, R. Thomale, K. P. Schmidt, and S. Dusuel, *Phys. Rev. B* **80**, 081104 (2009).
- [50] J. Nasu, Y. Kato, J. Yoshitake, Y. Kamiya, and Y. Motome, *Phys. Rev. Lett.* **118**, 137203 (2017).
- [51] J. Ashkin and E. Teller, *Phys. Rev.* **64**, 178 (1943).

Supplemental Material

Trick of “fictitious Majorana zero mode”

Our derivation of $\hat{H}_{g,\sigma}$ in the main text assumes an even number of rows in the square lattice of Majorana fermions. Because of the open boundary in the **b** direction, this means there are an odd number of plaquettes in this direction. However, since the low T phase induces a modulation of energy density associated with the plaquette interaction g , a particular type of the modulation is favored in this setup, even if there are an even number of plaquettes in the **a** direction. To avoid resulting finite size effect in the QMC simulation, we consider the lattice with an even number of plaquettes, hence, an odd number of rows of Majorana fermions, also in the **b** direction [Fig. S1(a)].

A faithful spin representation can be derived also in this case. To combine the Majorana fermions in pairs properly, we add an additional row of fictitious MZMs as shown in Fig. S1(b). These fictitious modes are neither coupled to the rest of the system nor hybridizing within themselves. Therefore, they simply contribute to a constant to the free energy. We then apply the JW transformation in the same way as described in the main text. The only difference in the final form of $\hat{H}_{g,\sigma}$ is that the horizontal J coupling for σ spins in the top row of the lattice is absent [Fig. S1(c)], because they correspond to interaction involving the fictitious modes, which do not exist. Finally, Fig. S1(d) illustrates the order parameter of the Majorana stripe state,

$$\hat{D}_\sigma = \frac{2}{L_a(L_b - 1)} \sum_{\mathbf{r}_\sigma \in \text{even (or odd)}} \left(\hat{\sigma}_{\mathbf{r}_\sigma + \mathbf{a}}^z \hat{\sigma}_{\mathbf{r}_\sigma + 2\mathbf{a}}^z - \hat{\sigma}_{\mathbf{r}_\sigma + 2\mathbf{b}}^x \hat{\sigma}_{\mathbf{r}_\sigma}^x \hat{\sigma}_{\mathbf{r}_\sigma + \mathbf{a} + 2\mathbf{b}}^x \hat{\sigma}_{\mathbf{r}_\sigma + \mathbf{a}}^x \right), \quad (\text{S1})$$

where L_a and L_b are the size of the lattice of σ spins in the horizontal and vertical directions, respectively.

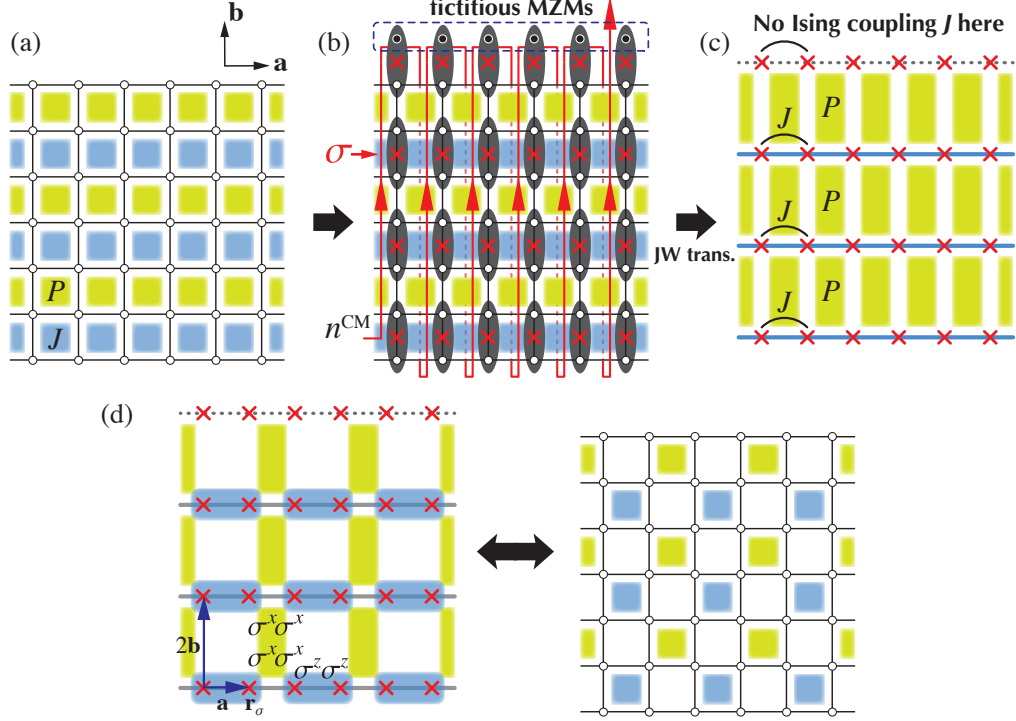


FIG. S1. (a) Lattice of Majorana fermions with an odd number of rows in the \mathbf{b} direction. (b) JW transformation. (c) Lattice of σ spins. (d) Illustration of the order parameter \hat{D}_σ [Eq. (S1)] and the relation with the representation in the Majorana fermion system.

Mean field theory

Here we present a zero-temperature mean-field calculation of the Majorana stripe phase. To consider the more general situations, we introduce two coupling constants g and g' for plaquettes on the even and odd-numbered rows, respectively, of the square lattice. The difference $\Delta g \equiv g - g'$ serves as a symmetry-breaking field. As a result of this explicit breaking of translation symmetry along the vertical direction, the unit cell is doubled. We thus label the Majorana fermions as $\hat{\gamma}_{\mathbf{r},s}$, where $s = 1, 2$ is the sublattice index and $\mathbf{r} = m\mathbf{a} + n(2\mathbf{b})$, with m, n being integers, denotes the Bravais lattice points. The interacting Majorana fermions are described by the following Hamiltonian

$$\begin{aligned} \hat{H} = & g \sum_{\mathbf{r}} \hat{\gamma}_{\mathbf{r},1} \hat{\gamma}_{\mathbf{r},2} \hat{\gamma}_{\mathbf{r}+\mathbf{a},1} \hat{\gamma}_{\mathbf{r}+\mathbf{a},2} + g' \sum_{\mathbf{r}} \hat{\gamma}_{\mathbf{r},2} \hat{\gamma}_{\mathbf{r}-2\mathbf{b},1} \hat{\gamma}_{\mathbf{r}+\mathbf{a},2} \hat{\gamma}_{\mathbf{r}+\mathbf{a}-2\mathbf{b},1} \\ & + it \sum_{\mathbf{r}} \left(\hat{\gamma}_{\mathbf{r},1} \hat{\gamma}_{\mathbf{r},2} + \hat{\gamma}_{\mathbf{r},2} \hat{\gamma}_{\mathbf{r}-2\mathbf{b},1} \right) + it \sum_{\mathbf{r}} \left(\hat{\gamma}_{\mathbf{r},1} \hat{\gamma}_{\mathbf{r}+\mathbf{a},1} - \hat{\gamma}_{\mathbf{r},2} \hat{\gamma}_{\mathbf{r}+\mathbf{a},2} \right) \end{aligned} \quad (\text{S2})$$

We first consider the most general mean-field decouplings of the quartic terms assuming no further breaking of the translation symmetry. Direct numerical calculation nonetheless shows that the diagonal term $\langle \hat{\gamma}_{\mathbf{r},1} \hat{\gamma}_{\mathbf{r}+\mathbf{a},2} \rangle$ vanishes identically in the self-consistent solution. We thus consider the following nonzero mean-field averages:

$$\Delta = i \langle \hat{\gamma}_{\mathbf{r},1} \hat{\gamma}_{\mathbf{r},2} \rangle, \quad \Delta' = i \langle \hat{\gamma}_{\mathbf{r},2} \hat{\gamma}_{\mathbf{r}-2\mathbf{b},1} \rangle, \quad \delta = i \langle \hat{\gamma}_{\mathbf{r},1} \hat{\gamma}_{\mathbf{r}+\mathbf{a},1} \rangle, \quad \delta' = i \langle \hat{\gamma}_{\mathbf{r},2} \hat{\gamma}_{\mathbf{r}+\mathbf{a},2} \rangle. \quad (\text{S3})$$

The resultant mean-field Hamiltonian is

$$\begin{aligned}
\hat{H}_{\text{MF}} = & -2ig\Delta \sum_{\mathbf{r}} \hat{\gamma}_{\mathbf{r},1} \hat{\gamma}_{\mathbf{r},2} - 2ig'\Delta' \sum_{\mathbf{r}} \hat{\gamma}_{\mathbf{r},2} \hat{\gamma}_{\mathbf{r}-2\mathbf{b},1} + N(g\Delta^2 + g'\Delta'^2) \\
& + i(g + g')\delta \sum_{\mathbf{r}} \hat{\gamma}_{\mathbf{r},2} \hat{\gamma}_{\mathbf{r}+\mathbf{a},2} + i(g + g')\delta' \sum_{\mathbf{r}} \hat{\gamma}_{\mathbf{r},1} \hat{\gamma}_{\mathbf{r}+\mathbf{a},1} - N(g + g')\delta\delta' \\
& + it \sum_{\mathbf{r}} (\hat{\gamma}_{\mathbf{r},1} \hat{\gamma}_{\mathbf{r},2} + \hat{\gamma}_{\mathbf{r},2} \hat{\gamma}_{\mathbf{r}-2\mathbf{b},1}) + it \sum_{\mathbf{r}} (\hat{\gamma}_{\mathbf{r},1} \hat{\gamma}_{\mathbf{r}+\mathbf{a},1} - \hat{\gamma}_{\mathbf{r},2} \hat{\gamma}_{\mathbf{r}+\mathbf{a},2})
\end{aligned} \tag{S4}$$

We next perform Fourier transform $\hat{\gamma}_{\mathbf{r},s} = \frac{1}{\sqrt{N/2}} \sum_{\mathbf{k}} \hat{\gamma}_{\mathbf{k},s} e^{i\mathbf{k} \cdot (\mathbf{r} + \mathbf{d}_s)}$, where $N/2$ is the number of unit cells and the basis vectors are $\mathbf{d}_{1,2} = \pm \mathbf{b}/2$. After introducing a basis vector $\hat{\Psi}_{\mathbf{k}} \equiv (\hat{\alpha}_{\mathbf{k}} \hat{\beta}_{\mathbf{k}})^T$ the mean-field Hamiltonian can be expressed as $\hat{H}_{\text{MF}} = \sum_{\mathbf{k}} \hat{\Psi}_{\mathbf{k}}^\dagger \mathcal{H}_{\text{MF}} \hat{\Psi}_{\mathbf{k}}$, where the matrix \mathcal{H}_{MF} is given by

$$\mathcal{H}_{\text{MF}} = -[t + (g + g')\delta] \sin k_x \tau^z - (g\Delta + g'\Delta' - t) \sin k_y \tau^x + (g\Delta - g'\Delta') \cos k_y \tau^y, \tag{S5}$$

Here $\tau^{x,y,z}$ are the Pauli matrices, and we have used the relation $\delta' = -\delta$ obtained from numerical solutions to simplify the expression. The mean-field spectrum is obtained by solving the above Hamiltonian self-consistently with Eq. (S3).

Figure S3 shows the order parameters as a function of the ratio g'/g with a fixed $g = 1$ for two different hybridization constant $t = 0.01$ and $t = 0.1$. The stripe order parameter D defined in the main text is given by $D = \Delta - \Delta'$. For small hopping $t = 0.01$ [Fig. S3(a)], the stripe order D remains finite as the system approaches the symmetric limit $g' \rightarrow g$. This result indicates the existence of a zero-temperature first-order transition at $\Delta g = 0$, discussed in the main text. As the hopping increases, the discontinuity in D at $\Delta g = 0$ is also reduced and eventually vanishes when $t > t_c \approx 0.65$. The mean-field band structure of Majorana fermions is shown in Fig. S4 for various ratios of g'/g with other parameters $g = 1$ and $t = 0.1$. Expressing $\mathcal{H}_{\text{MF}}(\mathbf{k}) = \sum_{m=x,y,z} a_m(\mathbf{k}) \tau^m$, the eigenenergy of the mean-field Hamiltonian is given by $\varepsilon_{\mathbf{k}}^\pm = \pm \sqrt{a_x^2 + a_y^2 + a_z^2}$, and always appears in \pm pairs. The energy gap corresponds to the minimum of $\varepsilon_{\text{gap}} = \min(\varepsilon_{\mathbf{k}}^+ - \varepsilon_{\mathbf{k}}^-)$ occurs at $\mathbf{k} = (0, 0)$, $(\pi, 0)$, $(0, \pi)$, and (π, π) . In the symmetric point $g = g'$, the spectral gap is related to the stripe order parameter

$$\varepsilon_{\text{gap}} = 2g(\Delta - \Delta') = g\Delta D. \tag{S6}$$

The energy gap as a function of the hybridization is shown in Fig. 5 of the main text. Importantly, the closing of the gap $\varepsilon_{\text{gap}} = 0$ for $t > t_c$ gives rise to a critical state with low-energy Dirac fermions; see Fig. S4.

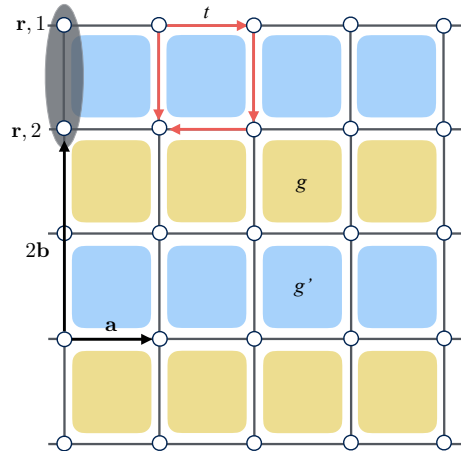


FIG. S2. Interacting Majorana fermions on a square lattice.

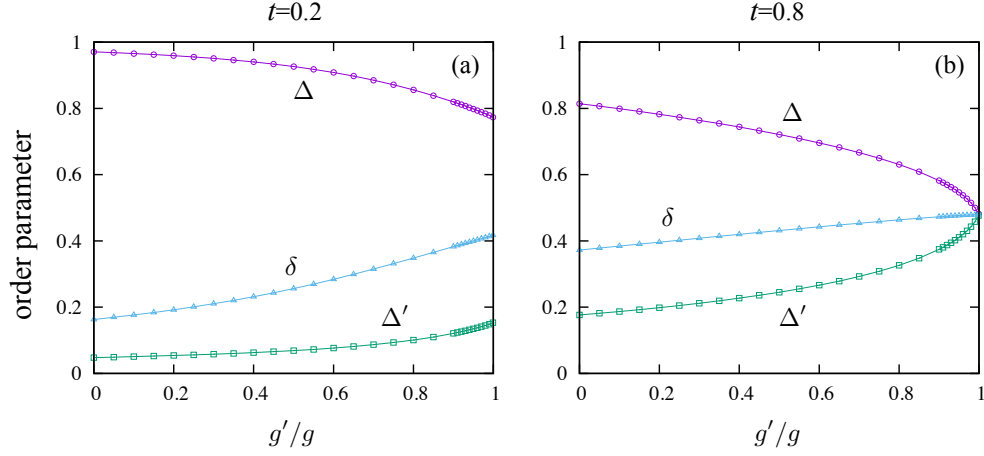


FIG. S3. Mean-field order parameters Δ , Δ' , and δ as a function of the ratio g'/g for (a) $t = 0.2$ and (b) $t = 0.8$. The coupling g is fixed $g = 1$.

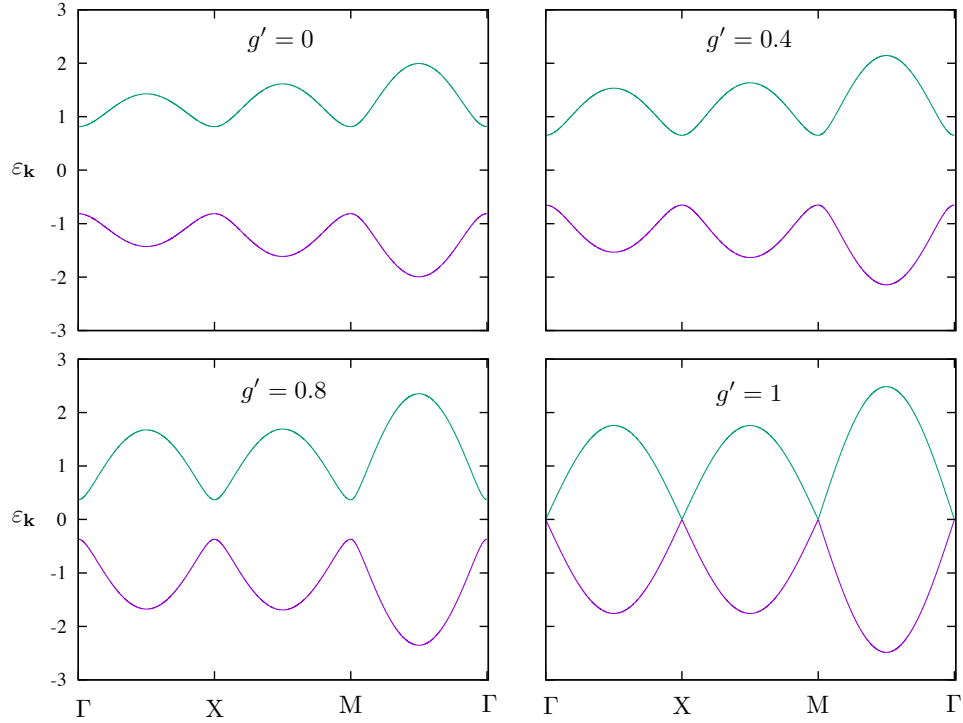


FIG. S4. Mean-field quasi-particle band structure with $g = 1$, $t = 0.8$.

Starting from large hybridization (focusing on the symmetric case $g = g'$), the Majorana stripe order occurs through a quantum phase transition that gaps out the Dirac points upon reducing the hopping t . A natural question is whether the gapped mean-field band structure is topologically nontrivial. To answer this question, we compute the Chern number of the bands explicitly for $t < t_c$. We first define a unit-length vector $\mathbf{m}(\mathbf{k}) = [a_z(\mathbf{k}), a_x(\mathbf{k}), a_y(\mathbf{k})]/\varepsilon_{\mathbf{k}}^+$. The spectral Chern number

is given by

$$\nu = \frac{1}{4\pi} \int \int \mathbf{m} \cdot \left(\frac{\partial \mathbf{m}}{\partial k_x} \times \frac{\partial \mathbf{m}}{\partial k_y} \right) dk_x dk_y = \text{integer}. \quad (\text{S7})$$

For simplicity, we introduce coefficients $C_{x,y,z}$ such that $\mathbf{m}(\mathbf{k}) = [C_x \sin k_x, C_y \sin k_y, C_z \cos k_y]/\varepsilon_{\mathbf{k}}^+$; these coefficients can be easily obtained by comparing with Eq. (S5). In our case, the integrand $\mathbf{m} \cdot \partial_{k_x} \mathbf{m} \times \partial_{k_y} \mathbf{m}$ evaluates to

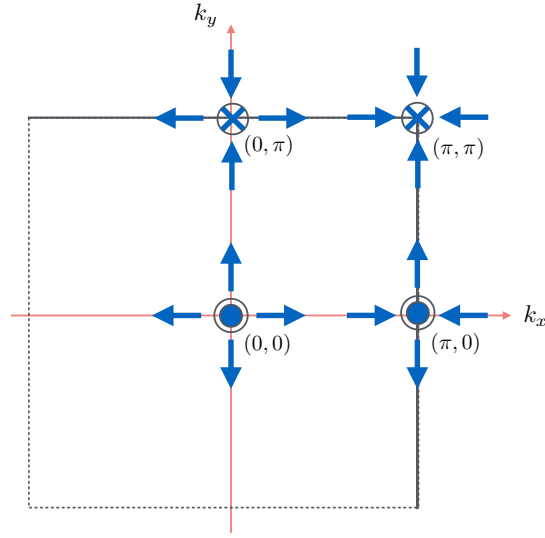


FIG. S5. The vector field in the vicinity of the four original Dirac nodes: $\mathbf{m} \approx (k_x, k_y, C_z)$ around $(0, 0)$, $\mathbf{m} \approx (-k_x, k_y, C_z)$ around $(\pi, 0)$, $\mathbf{m} \approx (k_x, -k_y, -C_z)$ around $(0, \pi)$, and $\mathbf{m} \approx (-k_x, -k_y, -C_z)$ around (π, π) .

$C_x C_y C_z \cos k_x / (\epsilon_{\mathbf{k}}^+)^3$. Consequently, the Chern number is zero, indicating a topologically trivial gapped phase. This result can also be understood by noting that the \mathbf{m} -vector maps the Brillouin zone to a unit sphere, and the Chern number is simply the winding number of this mapping. In the gapped phase (say $C_z = gD > 0$), the neighborhood around the original Dirac nodes $(0, 0)$ and $(\pi, 0)$ is mapped to the north hemi-

sphere, while that around the other two nodes is mapped to the south hemisphere; see Fig. S5. Within each hemisphere, the winding number is determined by the in-plane vorticity of the two nodes. In our case, the two Dirac nodes within the same hemisphere have opposite vorticity ± 1 , hence the net winding number is zero.